DOI: 10.1002/cphc.201000507

MRI Thermometry Based on Encapsulated Hyperpolarized Xenon

Franz Schilling,*[a, b] Leif Schröder,[a] Krishnan K. Palaniappan,[a] Sina Zapf,[b] David E. Wemmer,[a] and Alexander Pines*[a]

A new approach to MRI thermometry using encapsulated hyperpolarized xenon is demonstrated. The method is based on the temperature dependent chemical shift of hyperpolarized xenon in a cryptophane-A cage. This shift is linear with a slope of 0.29 ppm °C^{-1} which is perceptibly higher than the shift of the proton resonance frequency of water (ca. 0.01 ppm °C^{-1}) that is currently used for MRI thermometry. Using spectroscopic imaging techniques, we collected temperature maps of a phantom sample that could discriminate by direct NMR detection between temperature differences of 0.1 °C at a sensor concentration of 150 μM. Alternatively, the xenon-in-cage chemical shift was determined by indirect detection using saturation transfer techniques (Hyper-CEST) that allow detection of nanomolar agent concentrations. Thermometry based on hyperpolarized xenon sensors improves the accuracy of currently available MRI thermometry methods, potentially giving rise to biomedical applications of biosensors functionalized for binding to specific target molecules.

Introduction

Noninvasive, accurate and spatially resolved temperature measurement in the human body is a desirable technology for many biomedical applications, including the monitoring of hyperthermic treatment of cancer and the detection of vulnerable atherosclerotic plaques.[1–5] The advantages of magnetic resonance imaging (MRI), including its noninvasiveness and the ability to image in any scan orientation with good spatial and temporal resolution, make it a promising candidate for temperature imaging.[6] Many magnetic resonance parameters that are inherently temperature sensitive have been studied including the proton resonance frequency (PRF), the diffusion coefficient (D), transverse and longitudinal relaxation times (T_1 and T_2) and temperature sensitive contrast agents.[7] The accuracy of conventional thermometry methods like PRF is limited due to low sensitivity and susceptibility artifacts.[5] While such techniques provide useful relative temperature measurements, absolute temperature information is advantageous for biomedical observation. MRI thermometry therefore remains a "…greatly anticipated technology for in vivo applications".[6] An approach to such absolute temperature measurements has been provided by the measurement of intermolecular zero-quantum coherences in vivo, a technique that works well in the presence of abundant fat and water protons.[8]

In this work we introduce xenon sensors as a temperature contrast agent for MRI thermometry to gain both high accuracy and sensitivity.[9] With xenon, high sensitivity can be achieved by hyperpolarization through spin exchange optical pumping that increases the equilibrium net spin polarization by three to four orders of magnitude.[10,11] The sensor used for this work consists of three major components: a cryptophane-A cage for hosting the xenon atom, a linker, and a peptide for sufficient water solubility (see Experimental Methods and Figure 1 in the Supporting Information).[12–14] Such sensors can also serve as biosensors when functionalized with a targeting group.[9]

In a sensor solution containing xenon, the noble gas equilibrates between a bound and unbound state with the cryptophane cage. The cage-bound lifetime is ≈40 ms in water at room temperature, the longitudinal relaxation time constant T_1 is ≈66 s in water at 9.4 T, and the frequency difference between the xenon-in-cage peak and xenon-in-water peak is more than 120 ppm.[9,15] Hence, the exchange of xenon between solution and the sensor is fast on the relaxation timescale and slow on the chemical shift timescale, which makes it suitable for hyperpolarized xenon chemical exchange saturation transfer (Hyper-CEST).[16]

The chemical shift of xenon in the cryptophane cages is also influenced by temperature, increasing linearly at a rate of 0.1 to 0.3 ppm K^{-1}.[14,17,18] The temperature dependence arises from

[a] F. Schilling,[+] Dr. L. Schröder,[$] K. K. Palaniappan, Prof. D. E. Wemmer, Prof. A. Pines
Lawrence Berkeley National Laboratory
Materials Sciences Division, Berkeley CA 94720 (USA)
Fax: (+1) 510-666-3768
E-mail: fschilling@tum.de
pines@berkeley.edu

[b] F. Schilling,[+] S. Zapf
University of Würzburg
Experimental Physics 5, 97074 Würzburg (Germany)

[+] Current address
Technical University München
Department of Chemistry and Zentralinstitut für Medizintechnik
85748 Garching (Germany)

[$] Current address
Campus Berlin Buch, Leibniz-Institut für Molekulare Pharmakologie
13125 Berlin (Germany)

Supporting information for this article is available on the WWW under http://dx.doi.org/10.1002/cphc.201000507.

both the increase in conformational flexibility of the cage molecule and the increase in location accessible by xenon in the cage at higher temperatures. Consequently, changes in the average deformation of the xenon electron cloud can induce changes in the average chemical shift. At higher temperatures, xenon is able to interact with higher potential energy areas of the cage, which are less shielded. The linear temperature dependence has been confirmed by theoretical models, calculating the shielding surface for a xenon atom in a cryptophane-A cage and simulating temperature effects by Monte-Carlo methods.[19]

Results and Discussion

Calibration

The chemical shift difference between the xenon sensor δ_1 (xenon-in-cage) and the xenon-in-water peak δ_2 (xenon-in-water) was determined between 25 °C and 45 °C in steps of 2 °C. All peaks were fitted with Lorentzian lineshapes. The absolute errors of the individual peak positions are less than 0.05 ppm. Linear regression gives a linear temperature response with a high correlation coefficient, $R=0.9997$, and a slope of 0.29 ppm °C^{-1} (see Figure 1 a). The sample temperature [Eq. (1)] was set with the spectrometer hardware (see Experimental Methods).

$$\delta_2[\mathrm{ppm}]-\delta_1[\mathrm{ppm}] = -0.29\ \mathrm{ppm}\,^{\circ}\mathrm{C}^{-1}\,T[^{\circ}\mathrm{C}] + 138.57\ \mathrm{ppm} \quad (1)$$

This calibration equation was used for all following temperature images. The reference peak is quantified once the chemical shift scale is set to the xenon-in-gas peak at 25 °C referenced to 0 ppm. The accuracy of temperature measurements with this method are not affected by drifts of the B_0 field since the method relies on a difference measurement between two peaks. Different solvent compositions would give different chemical shift differences $\Delta\delta=\delta_2-\delta_1$ which has to be considered in chemical environments different from water, for example, for lipid environments particularly important for in-vivo applications. Changes in pH did not influence the chemical shift xenon encaged in our particular construct.

The cryptophane-A complex characterized in this work has a relatively high temperature dependence. Recently, 12 different cryptophane complexes dissolved in 1,1,2,2-[D_2]tetrachloroethane were examined with regard to their temperature dependence of the chemical shift.[22] These cryptophane cages were sorted in 4 different groups according to their temperature dependence (ca. 0.084 ppm °C^{-1} to 0.3 ppm °C^{-1}).

Direct Temperature Imaging

The goal of temperature-imaging based on hyperpolarized encapsulated xenon is to spatially detect the chemical shift of the xenon-in-cage peak relative to a reference peak that insignificantly changes its chemical shift with temperature, for example, the xenon-in-water peak (shifts with 0.03 ppm K^{-1}).[20] Chemical shift imaging is a method that maps spectral information, providing a way to display changes in chemical shift with respect to each location in an object or subject of interest.[23] In this way, the xenon-in-cage chemical shift is detected directly in each voxel and can be related to the mean temperature of each voxel. Images at four different constant temperatures, between 25 °C and 28 °C in steps of 1 °C, were collected in a 5 mm probe containing a 150 μM sensor solution (see Figure 1 b).

In a follow-up experiment with the same experimental parameters, the set temperature was increased by 0.1 °C per step, in a series ranging from 26.0 °C to 26.5 °C (see Supporting Information Figure 3). Even though a temperature difference of 0.1 °C is at the limit of the accuracy of the spectrometer's variable temperature unit, this slight increase could be detected. The total acquisition time for each of these 4×4 CSI temperature images was 4 min 48 s. This timescale might be sufficient for observational studies of hyperthermic heating procedures or cooling processes with high temperature accuracy.

Temperature imaging based on encapsulated hyperpolarized xenon sensors was also demonstrated in a more demanding setup: a temperature gradient

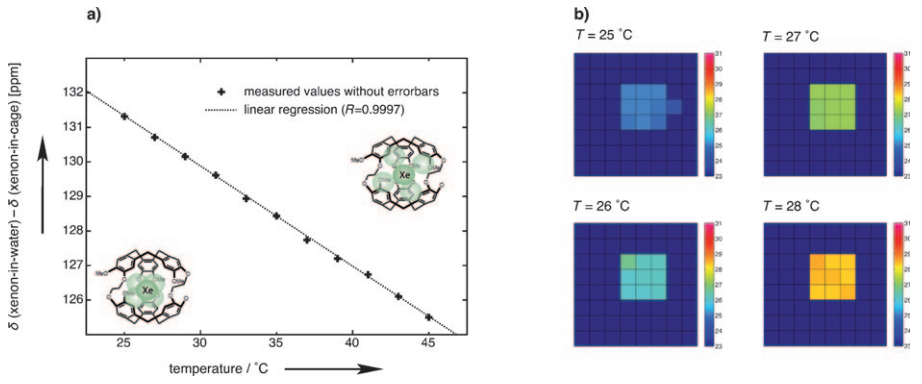

Figure 1. Temperature calibration. a) The relationship between the temperature and the difference in chemical shift between xenon-in-cage and xenon-in-water at a sensor concentration of 150 μM. With increasing temperature, the peak difference shifts downfield with a slope of 0.29 ppm °C^{-1}. This phenomenon arises from xenon atoms sampling a larger volume inside the cages, as indicated in the figure. At each temperature, the peaks were fitted with a Lorentzian curve based on a least squares algorithm. Absolute errors of the peak positions are smaller than 0.05 ppm (and therefore too small to be displayed). b) Maps showing the detected temperature of a 5 mm NMR tube containing a 150 μM sensor solution at homogeneous temperatures. The sample was bubbled with hyperpolarized xenon gas for 10 s, after which a 3 s wait time was applied before acquisition. As the temperature was increased from 25 °C to 28 °C in steps of 1 °C, CSI images were taken with one scan and an acquisition time of 4 min 48 s. The temperature was only calculated for voxels that showed an integrated peak height twice that of noise.

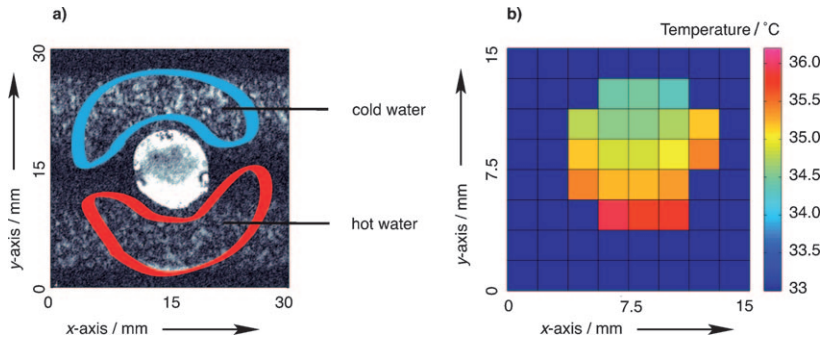

Figure 2. Detection of a temperature gradient. a) Gradient echo image of the temperature gradient phantom with continuous flow of hot or cold water in the surrounding compartments. The image matrix is 256×256, a 5 mm slice was selected, and the image was acquired with 4 scans during flow. b) Temperature map of the inner compartment of the temperature gradient phantom. The image was collected with 32 scans and a total acquisition time of 2 h 10 min. Signal averaging was necessary since the SNR of xenon-in-cage was too low to detect with a single scan. The FOV is 15 mm×15 mm, the image matrix size is 4×4 and extended to 8×8 after zero filling. The range of the gradient was found to be 2 °C as confirmed by independent optical thermometry (T1™ Temperature Sensor, Neoptix Inc., Canada).

phantom was built to allow the formation of a linear temperature gradient emanating from inside the inner compartment (see Experimental Methods and Supporting Information Figure 2). Hyperpolarized xenon gas was dissolved in water by bubbling through microcapillaries in the inner compartment of the temperature gradient phantom.[24] Even though the temperature gradient did not reach a state of thermal equilibrium, due to the bubbling in the inner compartment, it was still detectable. The solution was bubbled for 10 s followed by a 5 s wait time allowing the bubbles to disperse before each acquisition. After allowing 5 s, for the effect of the gradient, the temperature distribution was detected in a thermal image (see Figure 2).

Indirect Temperature Imaging

Some applications might require relatively low concentrations, in which case the reduced sensitivity for direct detection of the cage peak can be overcome by indirect detection with Hyper-CEST. This method provides a large increase in sensitivity, allowing the detection of low μM to nM concentrations. Functionalized biosensors have been detected at concentrations of 10 nM, a sensitivity gain of 4000-fold compared to direct detection.[20,21] With this technique, temperature imaging becomes possible at very low concentrations of the sensor. Such thermometry via indirect detection of the xenon-in-cage chemical shift can be achieved through selective saturation with low bandwidth continuous wave (cw) pulses at different offset frequencies, swept in a range including the xenon-in-cage center frequency. Each saturation offset gives a characteristic saturation effect, with a maximum saturation effect when the saturation offset is tuned exactly to the xenon-in-cage center frequency. This type of acquisition creates an array of different residual longitudinal (z) magnetization, and therefore is termed a z-spectrum. Temperature imaging can be achieved through narrow bandwidth saturation pulses at different offset frequencies, stepped through the xenon-in-cage frequency range. A saturation pulse with a cw pulse shape with the lowest possible power setting, corresponding to $B_1 = 0.58$ μT, results in an effective pulse bandwidth of 18 Hz. This bandwidth was determined experimentally by saturating at different offsets around the xenon-in-water peak. Fitting a Lorentzian to the acquired z-spectrum yields the effective bandwidth of the saturation pulse. This pulse was applied for a saturation time, t_{sat}, of 1 s.

Next, indirect temperature imaging was demonstrated using a setup with two 10 mm NMR tubes that were both refreshed continuously by hyperpolarized xenon gas (see Experimental Methods and Figure 3c). Each tube was held at a constant temperature by running water through external tubings at 22 °C and 35 °C respectively (like a heating/cooling jacket). Figures 3a and b show a xenon spectrum of the complete sample volume after 128 scans. Both phantoms contained 150 μM concentrated sensor solution. Two xenon-in-cage peaks appear, each related to a different temperature in the sample volume. With this setup, a series of CSI images for different saturation offsets was taken. For each voxel, the offset with maximum saturation effect can be identified and related to a mean temperature of this voxel. This way, a full temperature map of the field of view can be created (see Figure 3d), clearly identifying a hot and a cold tube. The step size for the offset sweep (0.3 ppm) corresponds to a temperature accuracy of 1 °C. However, decreasing the frequency step size or the effective saturation bandwidth can improve temperature accuracy. In both cases, the number of acquisitions is increased in order to scan the same temperature range.

Since the acquisition time for a 4×4 classical CSI matrix with selective saturation is about 5 min, the acquisition of a z-spectrum with 10 different offsets takes 50 min, which is too long for most thermometry applications. In principal, a long chemical shift imaging acquisition scheme with full FID readout is not necessary for indirect temperature detection, since the chemical shift of the cage is determined by the minimum in a z-spectrum. Therefore, a fast imaging sequence using a low-flip angle FLASH acquisition can speed up indirectly detected temperature images and would allow for a higher spatial and temporal resolution (implementation of this method is currently in progress; for consistency, we only compare CSI results in this paper).

CSI imaging sequences can be made much faster; if the signal-to-noise ratio (SNR) of the observed peaks is sufficiently high, further increases in the temporal resolution are possible. Given the fact that the polarization of xenon was only 2.6% and no isotopically enriched xenon was used, under optimum conditions (polarization of ≈50% and isotopically enriched xenon) the SNR can be increased by up to two orders of mag-

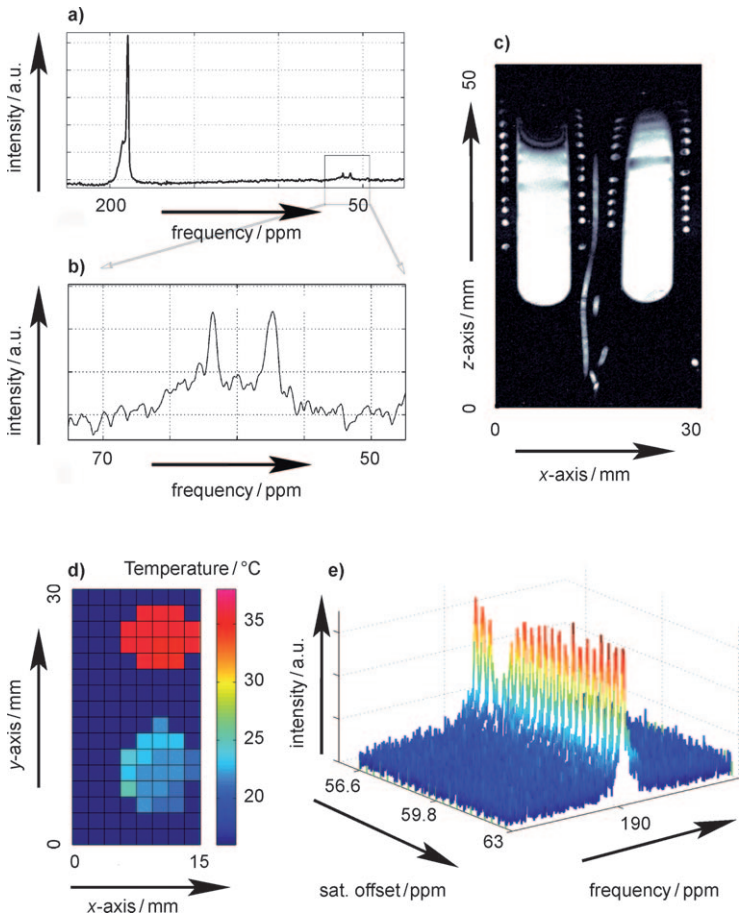

Figure 3. Indirect temperature detection using Hyper-CEST. a) Unlocalized xenon spectrum of a 150 μM sensor solution taken with 128 scans. The intense xenon-in-water peak is set as a chemical shift reference at 189.4 ppm and split due to poor field homogeneity, while two cage peaks related to two different sample temperatures are visible around 60 ppm. b) A zoomed view of the xenon-in-cage peaks. c) Coronal ^{1}H gradient echo image with a 1 mm slice thickness showing the two glass tubes filled with sensor solution. 1/8 inch tubing is wrapped around the glass phantoms with continuous water flow to hold phantoms at 22 °C or 35 °C respectively. d) Temperature map, created by determining the offset with maximum saturation which identifies the chemical shift of xenon-in-cage. e) As an example, the *z*-spectrum of the center voxel (see Figure 3 d) of the cold tube is shown. The saturation offset was swept over a range of 6.5 ppm with a step size for the offset of 0.3 ppm. The CSI datasets were taken with a 30 mm × 15 mm field of view and a 8 × 4 matrix (zero-filled to 16 × 8) in a transverse direction and 50 mm slice thickness. A cw saturation pulse with $B_1 = 0.58$ μT was applied for 5 s at each saturation offset. All CSI images were combined to create a *z*-spectrum for each voxel in the image matrix.

nitude. In this case, FLASH-based or EPI-based fast CSI sequences could substantially decrease the acquisition time, making direct imaging both a fast and accurate MRI thermometry method.[23]

Nevertheless, there are still challenges for in vivo studies: Xenon has to be delivered to areas of interest in the body either by uptake through the lungs or injection of carrier solutions into the blood. Accumulation of the cryptophane in the area of interest in the body can be achieved by functionalizing the cage to bind to a specific target.[16] In the case of xenon biosensors, the accumulation of the cryptophane in the body and the delivery of xenon for imaging can be separated in time. Beyond the continuous xenon administration, the sensor needs to accumulate in the area of interest at high enough concentrations over the course of an experiment. Unlike other contrast agents, xenon crosses the blood-brain barrier.

Conclusions

In this work, we demonstrate a new MRI thermometry method based on encapsulated hyperpolarized xenon, facilitating the detection of temperature changes of 0.1 °C. Temperature mapping using the xenon sensors offers high temperature accuracy and absolute temperature detection at low (150 μM, direct imaging) and ultralow agent concentrations (10 nM, indirect imaging). Taken together, encapsulated hyperpolarized xenon is a promising probe for accurate MRI thermometry, with a bright outlook for improved sensitivity and accuracy.

Experimental Section

Sensor Construct: All chemical reagents were of analytical grade, obtained from commercial suppliers, and used without further purification unless otherwise noted. Reversed-phase HPLC was performed using a Rainin Instruments Dynamax SD-200 system equipped with a Varian UV-Vis detector (model 345) and a Microsorb C18 analytical column (4.6 × 250 mm) at a flow rate of 1 mL min^{-1}, a semipreparative column (10 × 250 mm) at a flow rate of 4 mL min^{-1}, or a preparative column (21.4 × 250 mm) at a flow rate of 20 mL min^{-1}. HPLC samples were filtered with a Pall Life Sciences Acrodisc CR 13 mm syringe filter equipped with a 0.2 μm PTFE membrane prior to injection.

The sensor (see Supporting Information Figure 1) was synthesized by first preparing the water solubilizing tetrapeptide, Lys-Glu-Glu-Glu-Glu, on Wang resin (100–200 mesh) using standard Fmoc solid-phase peptide synthesis (SPPS) with *N*α-Fmoc protected amino acids, *N*,*N*- diisopropylethylamine, and HOBT/HBTU ester activation in *N*,*N*-dimethylformamide (DMF). A 5 fold excess of amino acid was used for the coupling steps, which involved gentle rotation for 1–2 h. Fmoc removal was achieved with 20% piperidine in DMF (1 × 20 min). Next, the linker was installed using *N*-Fmoc-6-aminohexanoic acid and the same SPPS conditions as above. Finally, the peptide was capped at the *N*-terminus using a 2.5 fold excess of the cryptophane-A acid cage and the same SPPS conditions as above. The sensor was cleaved for 2.5 h using trifluoroacetic acid:water:triisopropylsilane (95:2.5:2.5) and precipitated with methyl *tert*-butyl ether. The crude product was purified by reversed-phase HPLC using a C18 column. ESI-HRMS: Calc. for $C_{87}H_{104}N_7O_{28}$ (M-H):1694.69, found 1694.43.

Temperature Gradient Phantom: The temperature gradient phantom consists of an inner glass tube (10 mm inner diameter) which is fused to an outer glass tube (30 mm outer diameter). The inner volume is flanked on each side by equivalent compartments that can be filled with water through tube connectors on the top and the bottom (see Supporting Information Figure 3). Hot tap water (≈42 °C) was flowed through one of the compartments while the

other is connected to cold tap water (≈18 °C), leading to a temperature gradient in the inner compartment. The inner glass tube has a Chem-Thread (Chemglass Life Science, NJ, USA) connector on the top that enables xenon dissolution by a capillary insert. The inner tube was tested at pressures up to 85 psi.

"Double-Bubble" Phantom**:** The "double-bubble" phantom consists of two 10 mm NMR tubes that can both be bubbled with xenon through capillary inserts. Bubbling of xenon is stopped before acquisition of the NMR signal by a triggered valve. Each glass tube was wrapped with 1/8 inch Teflon tubing which was connected to a water loop of either hot or cold water, leading to a stable temperature of each of the glass tubes.

Xenon MRI Experiments: All datasets were collected on a 7.05 T NMR Varian Unity Inova spectrometer (Varian, Palo Alto, CA) equipped with a gradient coil assembly (Resonance Research Inc., Billerica, MA) for imaging experiments. Probes with two resonance circuits, tunable to both the xenon and proton Larmor frequency (Varian, Palo Alto, CA), were used to excite and detect the xenon NMR signal. The sample bore diameters of the probes are 5 mm and 30 mm. The 5 mm probe has a closed bore, whereas the 30 mm probe is open to the bottom allowing easy feedthrough of tubing for the temperature gradient phantom. The 5 mm probe has a variable temperature unit (VT), which allows regulation of the sample temperature by controlled airflow around the sample. The temperature is read out via a thermocouple. The VT has an accuracy of ± 0.1 °C in the temperature range used. To generate hyperpolarized xenon, a commercial polarizer was used (XenoSpin, Amersham Health, Durham, NC). A gas mixture of 2% natural isotope abundance xenon (Airgas, Inc.) 88% helium, 10% nitrogen flowed through the optical cell with its flow monitored by a mass-flowmeter. The diode laser with 50 W cw output is line-narrowed (Brightlock™ Ultra-100™, QPC Lasers Inc., Sylmar, CA, USA) with a center frequency adjustable by diode temperature to match the rubidium D_1 transition at 794.8 nm. With a flow rate of 0.4 SLM, polarization levels of typically 2–4% were achieved.

Acknowledgements

This work was supported by the Director, Office of Science, Office of Basic Energy Sciences, Materials Sciences and Engineering Division, of the U.S. Department of Energy under Contract No. DE-AC02–05CH11231. F.S. acknowledges support from Studienstiftung des deutschen Volkes. L.S. acknowledges support from the Deutsche Forschungsgemeinschaft through Emmy Noether Fellowships (SCHR 995/1-1 and SCHR 995/2-1) and by the European Research Council through Starting Grant BiosensorImaging under ERC Grant Agreement No. 242710. F.S. thanks Prof. Peter M. Jakob for scientific support. We would like to thank Prof. Matthew B. Francis for helpful discussions on sensor construction.

Keywords: imaging agents · NMR spectroscopy · sensors · thermometry · xenon

[1] B. Quesson J. A. de Zwart, C. T. W. Moonen, *J. Magn. Reson. Im.* **2000**, *12*, 525 – 533.
[2] A. Jordan, P. Wust, H. Fähling, W. John, A. Hinz, R. Felix, *Int. J. Hyperthermia* **1993**, *9*, 51 – 68.
[3] W. Wlodarczyk, M. Hentschel, P. Wust, R. Noeske, N. Hosten, H. Rinneberg, R. Felix, *Phys. Med. Biol.* **1999**, *44*, 607 – 624.
[4] W. Casscells, B. Hathorn, M. David, T. Krabach, W. Vaughn, H. McAllister, G. Bearman, J. Willerson, *Lancet* **1996**, *347*, 1447 – 1449.
[5] S. Zhang, C. R. Malloy, A. D. Sherry, *J. Am. Chem. Soc.* **2005**, *127*, 17572 – 17573.
[6] V. Rieke, K. B. Pauly, *J. Magn. Reson. Im.* **2008**, *27*, 376 – 390.
[7] G. A. Webb, Annual Reports on NMR Spectroscopy, **2002**.
[8] G. Galiana, R. T. Branca, E. R. Jenista, W. S. Warren, *Science* **2008**, *322*, 421.
[9] M. M. Spence, S. M. Rubin, I. E. Dimitrov, E. J. Ruiz, D. E. Wemmer, A. Pines, S. Q. Yaol, F. Tian, P. G. Schultz, *Proc. Natl. Acad. Sci. USA* **2001**, *98*, 10654 – 10657.
[10] B. M. Goodson, *Concepts Magn. Reson.* **1999**, *11*, 203 – 223.
[11] B. M. Goodson, *J. Magn. Reson.* **2002**, *155*, 157 – 216.
[12] P. Berthault, G. Huber, H. Desvaux, *Prog. Nucl. Magn. Reson. Spectrosc.* **2009**, *55*, 35 – 60.
[13] K. Bartik, M. Luhmer, J. P. Dutasta, A. Collet, J. Reisse, *J. Am. Chem. Soc.* **1998**, *120*, 784 – 791.
[14] T. Brotin, J. Dutasta, *Chem. Rev.* **2009**, *109*, 88 – 130.
[15] A. Bifone, Y.-Q. Song, R. Seydoux, R. Taylor, B. Goodson, T. Pietrass, T. Budinger, G. Navon, A. Pines, *Proc. Natl. Acad. Sci. USA* **1996**, *93*, 12932 – 12936.
[16] L. Schröder, T. Lowery, C. Hilty, D. E. Wemmer, A. Pines, *Science* **2006**, *314*, 446 – 449.
[17] M. M. Spence, E. J. Ruiz, S. M. Rubin, T. J. Lowery, N. Winssinger, P. G. Schultz, D. E. Wemmer, A. Pines, *J. Am. Chem. Soc.* **2004**, *126*, 15287 – 15294.
[18] T. J. Lowery, S. Garcia, L. Chavez, E. J. Ruiz, T. Wu, T. Brotin, J.-P. Dutasta, D. S. King, P. G. Schultz, A. Pines, D. E. Wemmer, *ChemBioChem* **2006**, *7*, 65 – 73.
[19] D. Sears, C. Jameson, *J. Chem. Phys.* **2003**, *119*, 12231 – 12244.
[20] L. Schröder, T. Meldrum, M. Smith, T. J. Lowery, D. E. Wemmer, A. Pines, *Phys. Rev. Lett.* **2008**, *100*, 257603.
[21] L. Schröder, L. Chavez, T. Meldrum, M. Smith, T. J. Lowery, D. E. Wemmer, A. Pines, *Angew. Chem.* **2008**, *120*, 4388 – 4392; *Angew. Chem. Int. Ed.* **2008**, *47*, 4316 – 4320.
[22] G. Huber, L. Beguin, H. Desvaux, T. Brotin, H. A. Fogerty, J.-P. Dutasta, P. Berthault, *J. Phys. Chem. A* **2008**, *112*, 607 – 624.
[23] R. Pohmann, M. von Kienlin, A. Haase, *J. Magn. Reson.* **1997**, *129*, 145 – 160.
[24] S.-I. Han, S. Garcia, T. J. Lowery, E. J. Ruiz, J. A. Seeley, L. Chavez, D. S. King, D. E. Wemmer, A. Pines, *Anal. Chem.* **2005**, *77*, 4008 – 4012.

Received: June 22, 2010
Published online on September 6, 2010

